

# Effect of Pre-existing Nano Sized Precipitates on Microstructure and Mechanical Property of Al-0.2wt% Sc Highly Deformed by ARB Process

E. Borhani<sup>1</sup>, H. Jafarian<sup>2</sup>

## Abstract

The effect of pre-existing nano sized precipitates on the mechanisms and rate of grain refinement has been investigated during the severe plastic deformation. A binary Al-0.2Sc alloy, containing coherent Al<sub>3</sub>Sc particles, of 3.62 nm in diameter has been deformed by accumulative roll bonding up to 10 cycles. The resulting deformed structures were quantitatively analyzed using electron backscattered diffraction and transmission electron microscope techniques, and the results have been compared to those obtained from a solution treated Al-0.2Sc alloy, deformed up to same accumulative roll bonding cycles. The fraction of high-angle grain boundaries and grain size in all materials was increased and decreased gradually with increasing equivalent strain, respectively. However, the Aged-ARB alloy had relatively higher fraction of high-angle grain boundaries and smaller grain size than those of ST-ARB specimens at the same accumulative roll bonding cycles. It was found in an Al-0.2%Sc alloy that starting microstructures significantly affect the formation of ultrafine grains during severe plastic deformation. It was shown that the small Al<sub>3</sub>Sc precipitates are more effective on microstructural evolution during accumulative roll bonding process. Existence of fine precipitates in the starting material greatly accelerated the microstructure refinement. In this regards some unique phenomena, including softening during severe plastic deformation and dissolution of pre-existing Al<sub>3</sub>Sc, were observed.

**Keywords:** Severe plastic deformation; Accumulative roll bonding (ARB); Ultrafine grains; Precipitation; Coherent interface; EBSD; High-angle boundaries (HAGBs)

## 1. Introduction

It has been clarified through a number of studies that severe plastic deformation (SPD) can produce bulky metals and alloys having ultrafine grained (UFG) microstructures [1-5]. SPD processing can be realized through a number of techniques, such as equal channel angular pressing (ECAP) [1], high-pressure torsion (HPT) [2] and accumulative roll bonding (ARB) [3]. In particular, the ARB allows us to accumulate very large strains into materials without changing the initial dimensions of the materials by repeating the processes of cutting the rolled sheet, stacking the cut segments of the rolled sheet to obtain the original thickness of the stack and rolling the new stacked sheets again. On the other hand, interactions between UFG microstructures and precipitation behaviors

have been scarcely studied. Precipitation hardening occurs during aging is an important and conventional way to strengthen materials, especially Al alloys [6-9].

Al-Sc alloys have recently aroused lots of interest because of their various advantages. Since fine Al<sub>3</sub>Sc precipitates in Al-Sc alloys are thermally stable due to low diffusivity of Sc atoms in Al, grain growth of the matrix grains is greatly inhibited and fine grained structures can be maintained [10-14]. Precipitation of Al<sub>3</sub>Sc also results in significant hardening, which is attributed to the coherency between fine Al<sub>3</sub>Sc precipitates and Al matrix [15]. The coherent precipitates would significantly affect the evolution of deformation microstructures and the change in mechanical properties in subsequent plastic deformation. It is well-accepted now that the

1- Department of Nanotechnology, Nano materials science and engineering group, Semnan University, Semnan, Iran.

2- School of Metallurgy and Materials Engineering, Iran University of Science and Technology (IUST), Tehran, Iran.

**Corresponding author:** E. Borhani, Department of Nano technology, Nano materials science and engineering group, Semnan University, Semnan, Iran.

Email: [ehsan.borhani@profs.semnan.ac.ir](mailto:ehsan.borhani@profs.semnan.ac.ir)

UFG structures develop in single-phase alloys deformed to high strain levels by SPD processes. However, the presence of second-phase particles could potentially have a significant effect on formation of UFG structures during SPD process. For example, it is expected that precipitates can increase the rate of dislocation generation and large local misorientation gradients. This can lead to an increased rate in the formation of HAGBs, so that ultrafine grains may be obtained at considerably lower strain than in precipitates-free alloys. At the same time, the second-phase particles can be effective in dislocation pinning [3, 15-17]. Microstructural properties of this alloy during accumulative roll bonding have been studied [15], however, little is known about the effect of  $\text{Al}_3\text{Sc}$  precipitates on the microstructural evolution during ARB in Al-0.2 Sc alloy. In the present study, effect of pre-existing  $\text{Al}_3\text{Sc}$  precipitates on the microstructure evolution and change in mechanical properties during SPD by accumulative roll bonding (ARB) was studied, using an Al-0.2 wt% Sc alloy.

## 2. Experimental

Sheets of Al-0.2 wt.% Sc alloy with 200 mm length, 60 mm width and 2 mm thickness were utilized in this research. Chemical composition of the studied alloy is shown in Table 1. The sheets were solution treated (ST) at 913 K for 24 h and immediately water-quenched. The average grain size of the ST sheets was 0.5  $\mu\text{m}$ . Some ST sheets were aged (A) at 573 K for 104 s to obtain fine  $\text{Al}_3\text{Sc}$  precipitates. These sheets are denoted as aged-sheets. Both solution treated and aged sheets were used as the starting materials for ARB process. A mill with two 310mm diameter rollers was used for rolling at room temperature with a rolling speed of 2.0 RPM. The same conditions were used for roll-bonding in the subsequent ARB process.

Figure 1 is a schematic illustration showing the principle of the ARB process [3]. In the ARB process, the cold-rolled sheets with 50% reduction having 1mm thickness were cut into half length, and then the contact surfaces of the sheets were degreased by acetone and wire-brushed by a stainless steel wire-brush before the two pieces of the sheets were stacked together and roll bonded by application of 50% reduction in each cycle. The roll-bonded sheets were immediately cooled in water. The same procedures were repeated up to 10 cycles including the first cold-rolling, which corresponded to the total equivalent strain of 8. It should be noted that, in the ARB process, the edge of the sheet commonly cracked and after each pass the cracked edges should be removed by cutting. Hereafter, the starting materials and the ARB processed samples by N cycles are expressed as ARB 0c and ARB Nc specimens, respectively. In addition, the ST sheets and Aged-sheets subjected to ARB process are denoted as ST-ARB and Aged-ARB specimens, respectively.

Sections perpendicular to the transverse direction (TD) of the sheets were used for microstructural observation. Electron backscattering diffraction (EBSD) analysis was carried out in a scanning electron

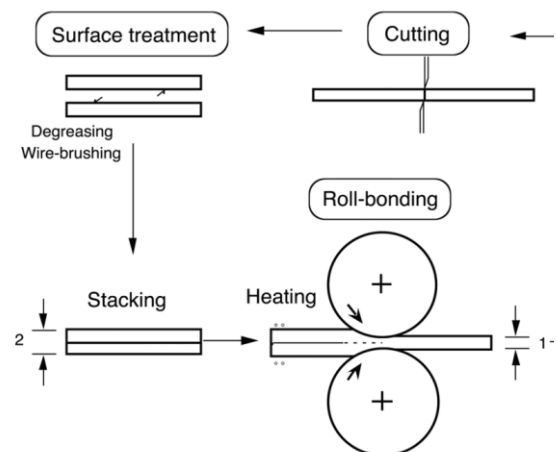


Fig. 1. Schematic illustration of ARB process.

Table 1. Chemical composition of the material used in the present study. (wt %)

Elements	Si	Cu	Mn	Mg	Cr	Zn	Ti	Sc	Al
Wt. %	0.016	0.004	0.001	0.001	0.003	0.001	0.002	0.188	Bal.

microscope with field emission type gun (FE-SEM; Philips XL30) operated at 15 KV. The specimens were mechanically and then electro-polished before the measurements. TEM observations were carried out using Hitachi H-800 operated at 200 kV. Thin foil specimens perpendicular to TD were mechanically polished to approximately 70  $\mu\text{m}$  in thickness and then electro-polished. Shimadzu HMW micro hardness tester was used for Vickers hardness measurement on the planes perpendicular to the normal direction (ND) of the Aged-ARB and ST-ARB sheets using a load of 0.098 kgf and a time period of 10 s at room temperature. X-ray diffraction (XRD) measurements were also performed using a Philips X'pert diffractometer on ST-ARB and Aged-ARB samples.

### 3. Result and Discussion

Dark field TEM images of aged specimen before the ARB process is shown in Fig. 2. The specimen aged at 573 K having fine spherical precipitates with mean particle size of 3.62 nm. The corresponding diffraction pattern indicates that they are L12  $\text{Al}_3\text{Sc}$  coherent to the Al matrix, keeping a particular orientation relationship.

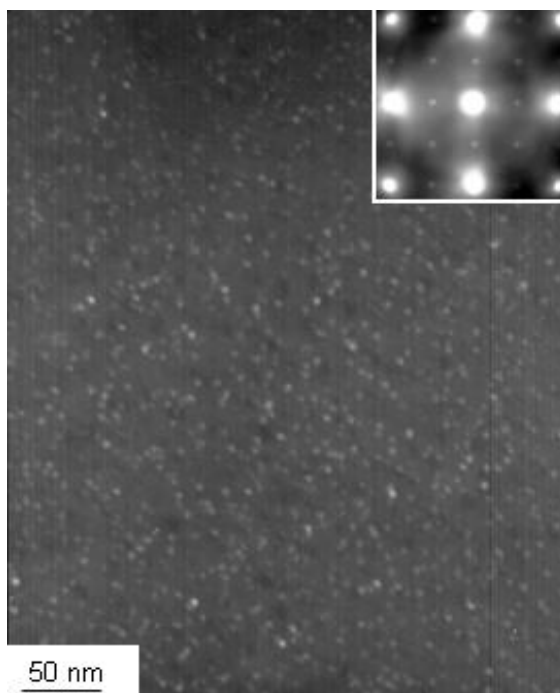


**Fig. 2.** TEM micrograph of 300°C aged specimen showing a dispersion of  $\text{Al}_3\text{Sc}$ .

Grain boundary maps of the ARB processed specimens obtained by EBSD measurement are presented in Fig. 3(a-f). Images in this figure are (a) ST-ARB 1c, (b) ST-ARB 5c, (c) ST-ARB 10c, (d) Aged-ARB 1c, (e) Aged-ARB 5c and (f) Aged-ARB 10c. In the boundary maps, high-angle boundaries (HAGBs) with misorientation angles larger than  $15^\circ$  are shown as green lines, while low-angle boundaries (LABs) with misorientation angles between  $2^\circ$  and  $15^\circ$  are shown as red lines. The boundaries having misorientation less than  $2^\circ$  were cut off, in order to remove the inaccuracy of EBSD measurements and analysis.

After 1 cycle of ARB process, the ST-ARB and Aged-ARB specimens (Fig. 3 (a, d)) show similar deformation microstructures composed of aligned dislocation boundaries (i.e. LAGBs) and small amount of HAGBs. The 5c-ARB processed specimens (Fig. 3 (b, e)) show the microstructures elongated to the rolling direction (RD). Some areas show small regions subdivided by high-angle boundaries, and the fraction of high-angle boundaries in the Aged-ARB specimen (Fig. 3 (e)) is larger than that in the ST-ARB specimen (Fig. 3 (b)). ST-ARB and Aged-ARB specimens after 10 cycles ARB process (Fig. 3 (c, f)) show the ultrafine lamellar structure elongated to RD, which are typical UFG structures fabricated by ARB process [18]. However, there are significant differences between the ST-ARB and Aged-ARB specimens. The microstructure of the Aged-ARB 10c (Fig. 3 (f)) shows more equiaxed grains than the ST-ARB 10c (Fig. 3 (c)). The mean boundary separation along ND and RD of the ST-ARB and Aged-ARB samples were evaluated and they are treated as the mean grain sizes ( $d_t$  and  $d_l$ ). Here, both HAGBs and LAGBs were counted as boundaries. The values of  $d_t$  for the ST-ARB 10c and Aged-ARB 10c specimens were  $0.37\mu\text{m}$  and  $0.24\mu\text{m}$ , while those of  $d_l$  were  $0.68\mu\text{m}$  and  $0.49\mu\text{m}$ , respectively. Furthermore, the Aged-ARB 10c specimen has larger amount of HAGBs (i.e.72%) than the ST-ARB 10c specimen (53%). The microstructure of the Aged-ARB 10c specimen was more homogeneous than that of

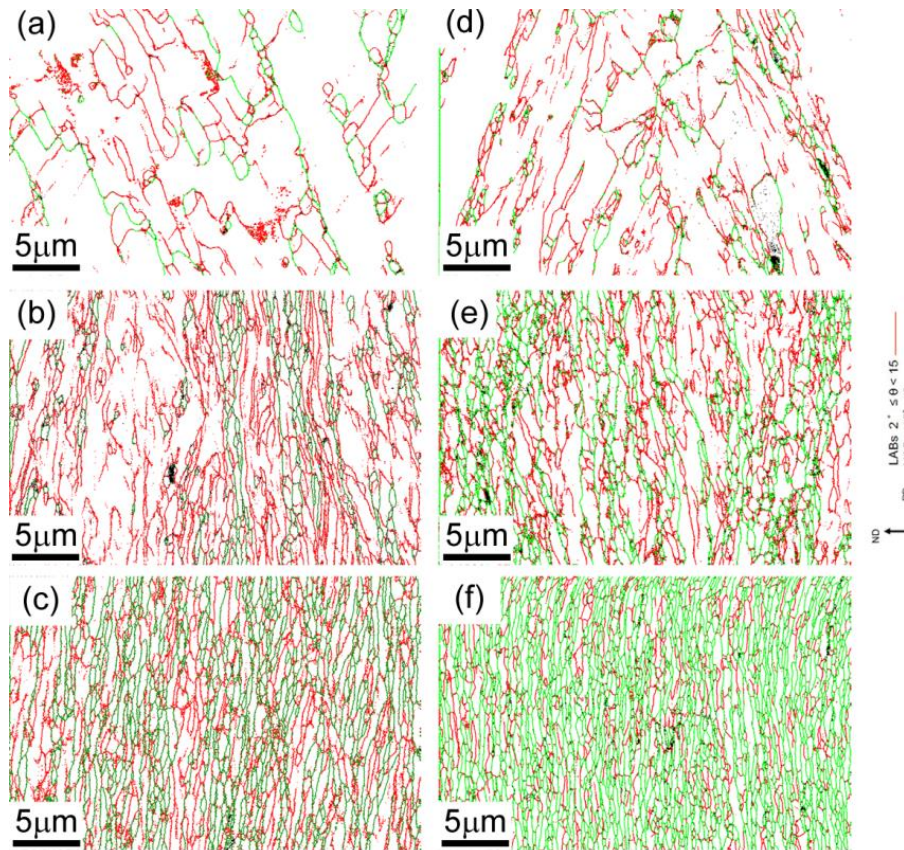


**Fig. 3.** Grain boundary maps obtained from EBSD measurement for the ST-ARB (a,b,c) Aged-ARB (d,e,f) specimens. ARB processed by 1 cycle (a,d), 5 cycles (b,e) and 10 cycles (c,f).

the ST-ARB 10c specimen. It is obvious that presence of fine precipitates in the starting material accelerates the generation of high angle grain boundaries in the Aged-ARB specimens.

Figure 4 shows the change in the grain size ( $dt$ ) as a function of ARB cycle number. The  $dt$  of the Aged-ARB and ST-ARB specimens decreases from over  $50 \mu\text{m}$  to about  $0.4 \mu\text{m}$  with increasing ARB cycle number up to  $N=5$ . Then, the  $dt$  of both specimens reduces

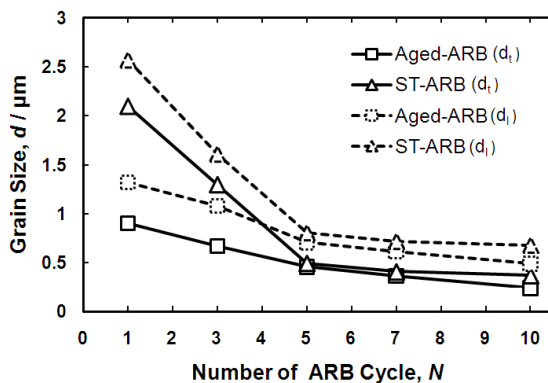


**Fig. 4.** Change in grain size as a function of the number of ARB cycles.

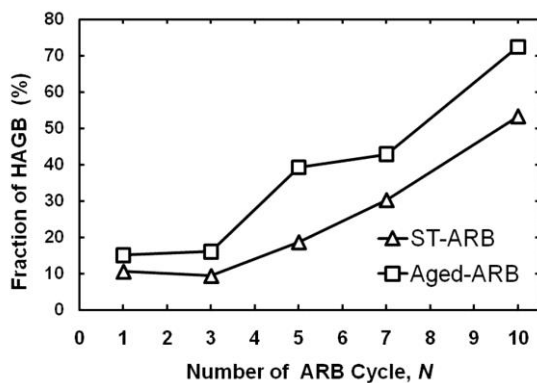
gradually to about  $dt=0.37 \mu\text{m}$  and  $dt=0.24 \mu\text{m}$ , respectively, with increasing the number of ARB cycle up to 10. Here, it is noteworthy that at early stages of the ARB process up to  $N=5$  the grain size of the Aged-ARB specimens is much smaller than that of the ST-ARB specimens, which indicates that the pre-existing precipitates have a significant effect on microstructure refinement. The precipitates in the Aged samples probably inhibit easy glide of dislocations as well as short range of grain growth during the ARB process. As a result, finer grains can be obtained in the Aged-ARB specimens than in the ST-ARB specimens.

It has been reported that precipitates can increase the rate of dislocation generation by encouraging the formation of Orowan and prismatic loops. In addition, precipitates inhibit the long-range migration of dislocations, so that uniform slip of dislocations become difficult and development of local deformation zones containing large

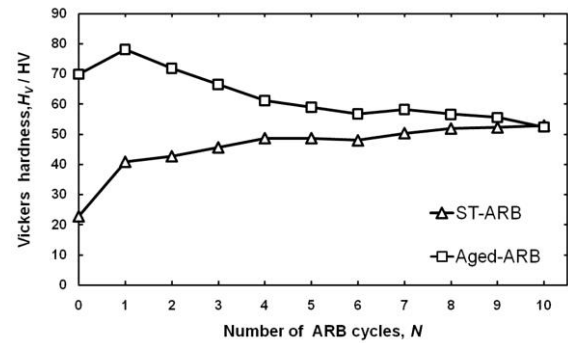
local misorientation gradients is promoted [3, 17, 19-21].

Fig. 3 demonstrates that grain subdivision takes place with increasing the number of ARB cycles in the Al-Sc alloy [22, 23]. From the EBSD data, the fraction of HAGBs (fHAGBs) is determined and plotted in Fig. 5 as a function of number of ARB cycles. With increasing number of ARB cycles, the fraction of high-angle grain boundaries monotonously increases in both specimens. The fHAGBs of the Aged-ARB specimens is always higher than that of the ST-ARB specimens. Finally, fHAGB of 72.4% and 53.3% were achieved in the Aged-ARB 10c and ST-ARB 10c specimens, respectively. It should be noted that even at 5 c (=4.0) and 7 c (=5.6), the microstructures are still somewhat inhomogeneous, where some regions include relatively large amount of LAGBs and the other regions show elongated UFG structures subdivided by HAGBs. The relatively slow UFG structure evolution in both specimens is probably due to the coarse initial grain size of the starting Al-Sc alloy.

Fig. 6 shows Vickers hardness of the ST-ARB and Aged-ARB specimens as a function of the number of ARB cycles. The hardness of three points for each specimen was considered for measurement of mean value of hardness. The results exhibited that the hardness of the starting materials (ARB 0c) is greatly varied. The Aged-ARB specimen showed much higher hardness (i.e. HV 70) than the ST-ARB specimen (i.e. HV 23). This was due to the presence of coherent  $\text{Al}_3\text{Sc}$  precipitates in the Aged specimens. Vickers hardness of the ST-



**Fig. 5.** Fraction of high angle grain boundaries as a function of the number of ARB cycles.



**Fig. 6.** Vickers hardness of the ST-ARB and Aged-ARB specimens as a function of ARB cycle number.

ARB specimen monotonously increases during the ARB process, which is a typical change in most ARB processed materials, and saturates around HV 52, assuming that the most strengthening in the precipitates-free specimen comes from Hall-Petch relation. On the other hand, Vickers hardness of the Aged-ARB specimen slightly increases at 1 cycle up to HV 78, and then monotonically decreases down to HV 52 at 10 ARB cycles. This increase of hardness in 1 ARB cycle is probably due to increase in dislocation density [24]. It is, however, noteworthy that the hardness of the Aged-ARB specimens is always higher than that of the ST-ARB specimen. These results indicate that the changes in mechanical behaviors of the Aged-ARB specimen are completely different from those of the ST-ARB specimen, which should be attributed to the difference in the starting microstructures including the presence of precipitates.

The microstructures of the Aged-ARB 9c and ST-ARB 10c specimens were observed by TEM and results are shown in Fig. 7. The ST-ARB 10c and Aged-ARB 9c specimens have similar lamellar structure. This is a typical ultra-fine structure formed by the ARB process. Some internal dislocations and subgrains within the grains were observed in the ST-ARB 10c specimen (Fig. 7 (a)). On the other hand, there are smaller numbers of dislocations in the Aged-ARB 9c specimen. It should be noted that fine  $\text{Al}_3\text{Sc}$  precipitates existed in the starting Aged specimens are hardly observed in Fig. 7 (b). However, X-ray diffraction measurements carried out in parallel clearly showed that there were still

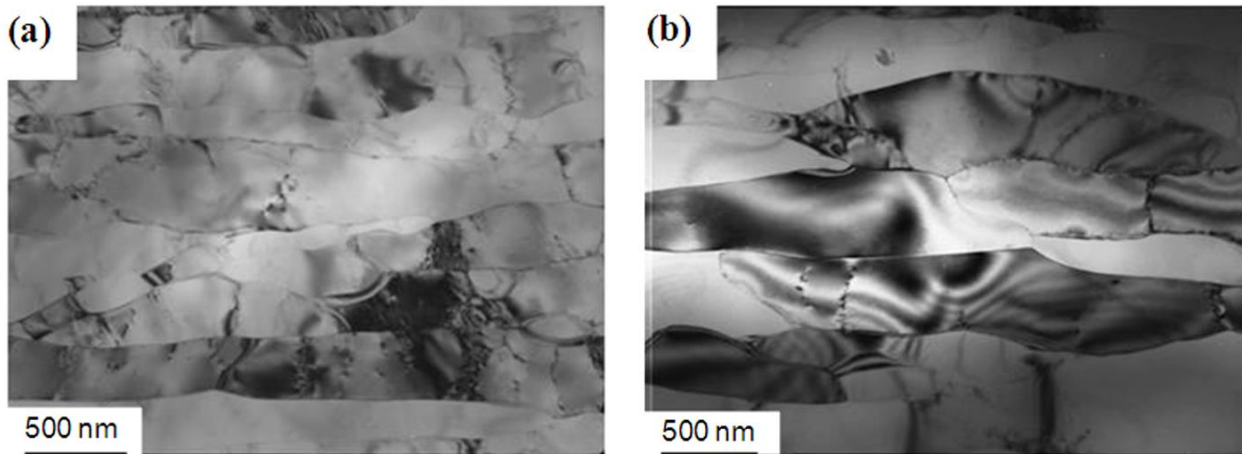


**Fig. 7.** TEM micrograph of (a) ST-ARB processed 10 c, (b) Aged-ARB 9 c specimens.

many  $\text{Al}_3\text{Sc}$  precipitates in the Aged-ARB 9c specimen. The reason why the precipitates were not observed in TEM (Fig. 7 (b)) might be due to the loss of coherency between  $\text{Al}_3\text{Sc}$  and the matrix during deformation. It is furthermore noteworthy that, from the integrated XRD peak intensity of  $\text{Al}_3\text{Sc}$  (Fig. 8), one can see that the volume fraction of  $\text{Al}_3\text{Sc}$  decreases with increasing the number of the ARB process. The result suggests that some of  $\text{Al}_3\text{Sc}$  dissolve during the ARB process, which has been reported in other alloy systems during severe plastic deformation [25-27]. This dissolution affects mechanical properties of specimens resulting in decrease of hardness as illustrated in Fig. 6. Such unique changes of precipitates would be the reason for the characteristic change in strength of the Aged-ARB specimens (Fig. 6).

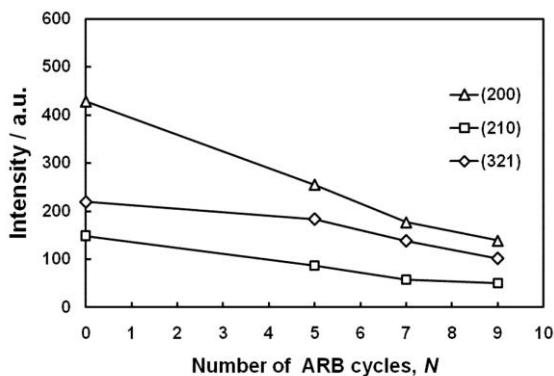


**Fig. 8.** Integrated intensity of  $\text{Al}_3\text{Sc}$  peaks in XRD of the Aged-ARB specimens as a function of the number of ARB cycles.

#### 4. Conclusions

An Al-0.2wt% Sc alloy was solution treated (ST) or aged to prepare two different starting microstructures. Both specimens were severely deformed up to an equivalent strain of 8.0 by accumulative roll bonding (ARB) process. The changes in microstructures and mechanical properties during the ARB were investigated. The main results obtained are as follows:

(1) Hardness of the ST-ARB specimen monotonously increased with increasing ARB strain, while the Aged-ARB specimens showed softening after 1 ARB cycle. This softening is a unique behavior of the pre-aged samples, which has not yet been reported previously. Hardness of the Aged-ARB specimens was always higher than that of the ST-ARB specimens.

(2) The specimens ARB processed by 10 cycles showed elongated ultrafine grain structures of which mean grain size was  $0.37 \mu\text{m}$  and  $0.24 \mu\text{m}$  for the ST and the Aged specimens, respectively. The fraction of high-angle grain boundaries was 53.28% and 72.4% for the ST and the Aged specimens, respectively, and the microstructure of the Aged specimen was finer and more homogeneous than that of the ST specimen.

(3) The present results clearly showed that the pre-aged starting microstructure significantly affected both microstructure evolution and change in mechanical properties. The formation of the UFG microstructure was

accelerated when the starting microstructure involved fine precipitates. TEM observation of the highly ARB processed specimens and XRD analysis suggested that the loss of coherency between Al<sub>3</sub>Sc precipitates and dissolution of Al<sub>3</sub>Sc are the possible reasons for the softening during ARB process in the Aged-ARB specimens.

## References

1. Valiev, R.Z., Langdon, T.G., *Prog. Mater. Sci.*, (2006), 51, 881.
2. Zhilyaev, A.P., Nurislamova G.V, Kim B.K, Baro´, M.D, Szpunar JA, Langdon, T.G., *Acta Mater.*, (2003), 51, 753.
3. Saito, Y., Utsonomiya, H., Tsuji, N, Sakai, T., *Acta Mater.*, (1999), 47(2), 579.
4. Jafarian, H.R., Borhani, E., *Iranian Journal of Materials Science & Engineering*, (2013), 10, 19.
5. Eivani A.R., Karimi Taheri A., *Journal of Materials Processing Technology*, (2007), 183, 148.
6. Røyset, J., Ryum, N. *Int. Mater. Rev.*, (2005), 50, 19.
7. Akamatsu, H., Fujinami, T., Horita, Z., Langdon, T.G., *Scr. Mater.* (2001), 44, 759.
8. Furukawa, M., Utsunomiya, A., Matsubara, K., Horita Z., Langdon, T.G., *Acta Mater.* (2001), 49, 3829.
9. Venkateswarlu, K., Pathak, L.C., Ray A.K., Das G, Verma P.K., Kumar M., Ghosh R.N., *Mater. Sci. Eng. A*, (2004), 383, 374.
10. Jindal, V., De, P.K., Venkateswarlu, K., *Mater. Letters*, (2006), 60, 3373.
11. Gubicza, J., Schiller, I., Chinh, N.Q., Illy, J., Horita, Z., Langdon T.G., *Mater. Sci. Eng. A*, (2007), 460–461, 77.
12. Marquis, E.A., Seidman, D.N., *Acta mater.* (2001), 49, 1909.
13. Gabriel, M. Novotny, Alan J. Ardell, *Mater. Sci. Eng. A*, (2001), 318, 144.
14. Min, B.K., Kim, H.W., Kang, S.B., *Materials Processing Technology*, (2005), 162–163, 355.
15. Quadir, M.Z., Ferry, M., Al-Buhamad, O., Munroe, P.R., *Acta Mater.*, (2009), 57, 29.
16. Quadir, M.Z., Al-Buhamad, O., Bassman, L., Ferry, M., *Acta Mater.*, (2007), 55, 5438.
17. Borhani, E., Jafarian, H.R., Adachi, H., Terada, D., Tsuji, N., *Mater. Sci. Forum*, (2011), 667-669, 211.
18. Huang, X., Kamikawa, N., Hansen, N., *Mater. Sci. Eng. A*, (2008), 493, 184.
19. F.J. Humphreys, M.G. Ardakani, *Acta Metallurgica* 42 (1994) 749.
20. P.B. Hirsch, F.J. Humphreys, In: A. Argon, Editor. *Physics of strength and plasticity* MIT Press (1969) 189.
21. P. J. Apps, M. Berta, P.B. Prangnell, *Acta Materialia* 53 (2005) 499.
22. Hansen, N., *Metall. Mater. Trans. A*. (2001), 32A, 2917.
23. Hansen, N., Junk Johnson D., *Phil. Trans. R. Soc. Lond. A*, (1999), 357, 1447.
24. Liu, H.S., Zhang, B., and Zhang G.P., *J. Mater. Sci. Technol.*, (2011), 27(1), 15.
25. Xu C., Furukawa M., Horita Z., Langdon T.G., *Acta Mater.* (2005), 53, 749.
26. Takata, N., Ohtake, Y., Kita, K., Kitagawa, K., Tsuji, N., *Scripta Mater.*, (2009), 60, 590.
27. Kima, W.J., Kima, J.K., Kimb, H.K., Park, J., Jeong, Y., *J. Alloys and Compounds* (2008), 450, 218.